

# The Analysis of Multijet Events Produced at High Energy Hadron Colliders

S. Geer

*Fermi National Accelerator Laboratory  
P.O. Box 500, Batavia, Illinois 60510*

T. Asakawa

*University of Tsukuba  
Tsukuba, Ibaraki 305, Japan*

PACS numbers: 12.38Qk, 13.85.-t, 13.85.Hd, 13.87.-a

## Abstract

We define and discuss a set of  $(4N - 4)$  parameters that can be used to analyse events in which  $N$  jets have been produced in high energy hadron-hadron collisions. These multijet variables are the multijet mass and  $(4N - 5)$  independent dimensionless parameters. To illustrate the use of the variables QCD predictions are presented for events with up to five jets produced at the Fermilab Tevatron Proton-Antiproton Collider. These QCD predictions are compared with the predictions of a model in which multijet events uniformly populate the  $N$ -body phase-space.

Submitted to Physical Review D.

# 1 Introduction

Large samples of events containing two or more jets have recently been recorded at the Fermilab Tevatron Proton-Antiproton Collider. Many of the observed events contain three-, four-, or even five-or-more jets [1]. A comprehensive analysis of these multijet events would provide an interesting test of perturbative Quantum Chromodynamics (QCD). In addition, a detailed understanding of the properties of multijet events produced in high energy hadron-hadron collisions is important, firstly because multijet production is expected to be prolific in future high luminosity running at the Fermilab Proton-Antiproton Collider and at the Large Hadron Collider at CERN, and secondly because an understanding of QCD multijet production is required to facilitate the search for more exotic processes producing multijet events. For example, a detailed understanding of the properties of six-jet events at the Fermilab collider is likely to be important in the near future for the study of  $t\bar{t}$  production and decay in the all hadronic channel.

In the past, elegant analyses of two-jet and three-jet production have been published by the UA1 [2, 3] and UA2 [4, 5] collaborations at the CERN  $S\bar{p}pS$  Collider and by the CDF [6, 7] and D0 [8] collaborations at the Fermilab Tevatron Collider. There have also been analyses of events with more than three jets [8, 9, 10]. However, the analyses of events with four or more jets have not used a simple set of independent variables that (i) span the multijet parameter space, (ii) make it simple to interpret the observed event distributions within the framework of perturbative QCD, and (iii) make it is easy to compare the characteristics of events having  $N$  jets with the characteristics of events having for example  $(N+1)$  jets. In this paper we discuss a set of multijet parameters that satisfy these criteria.

In choosing a set of multijet variables that span the multijet parameter space it should be noted that we can completely define a system of  $N$  particles in the  $N$ -body rest-frame by specifying  $4N$  independent parameters, for example the  $4N$  components of four-momentum. The  $N$ -body system would then be overspecified since momentum conservation provides us with three constraints. Furthermore, we can rotate the  $N$ -body system about the incoming beam direction without losing any interesting information. Therefore, to describe the system we need only specify  $(4N - 4)$  parameters. We will take these parameters to be the  $N$ -body mass and  $(4N - 5)$  additional variables. We therefore introduce and discuss a set  $(4N - 5)$  dimensionless variables which, with the addition of the multijet mass, span the multijet parameter space. Our  $(4N - 5)$  multijet variables will provide a simple framework within which the properties of multijet events can be compared with QCD predictions. To illustrate the use of these variables we will compare predictions for the population of events in the multijet parameter space obtained from QCD matrix element calculations with the corresponding predictions from QCD parton shower Monte Carlo calculations, and from a model in which the events are uniformly distributed over the available phase-space. The QCD and phase-space calculations are described in section 2. In section 3 the analysis of two-jet events

is briefly discussed. The standard three-jet variables are reviewed and extended in section 4. Four-jet and five-jet variables are introduced and discussed in sections 5 and 6. In section 7 the generalization of the multijet parameters to describe topologies with more than five jets is discussed. Finally, a summary is given in section 8.

## 2 QCD and Phase-Space Predictions

To illustrate the use of our multijet variables we will present and discuss various predictions for the distribution of multijet events in the multijet parameter space. In particular we will consider two-jet, three-jet, four-jet, and five-jet events produced at the Fermilab Proton-Antiproton Collider operating at a center of mass energy of 1.8 TeV, and compare predictions obtained from: (a) the HERWIG [11] QCD parton shower Monte Carlo program, (b) the NJETS [12] Leading Order (LO) QCD  $2 \rightarrow N$  matrix element Monte Carlo program, and (c) a model in which events are distributed uniformly over the available N-body phase-space.

### 2.1 Jet definitions and selection criteria

The QCD and phase-space model predictions depend upon the algorithm used to define jets and the selection criteria used to define the data sample. To illustrate the use of our multijet variables we will take as an example jet definitions and event selection criteria recently used by the CDF collaboration to define a multijet data sample recorded at the Fermilab Proton-Antiproton Collider [1]. Our predictions will therefore be for an existing data sample. Following the CDF prescription, jets are defined such that they satisfy the following:

- (i) Jet transverse energy  $E_T > 20$  GeV, where  $E_T \equiv E \sin \theta$ ,  $E$  is the jet energy, and  $\theta$  is the angle between the jet and the beam direction in the laboratory frame,
- (ii)  $|\eta| < 3$ , where the jet pseudorapidity  $\eta \equiv -\log \tan(\theta/2)$ , and
- (iii) jet-jet separation  $\Delta R > 0.9$ , where  $\Delta R \equiv (\Delta\eta^2 + \Delta\phi^2)^{1/2}$ , and  $\Delta\eta$  and  $\Delta\phi$  are the differences in pseudorapidity and azimuthal angle between the two jets.

With these jet definitions, the multijet event sample is defined by selecting events that satisfy the following:

- (a) Total transverse energy  $\sum E_T > 420$  GeV, where the sum is over all jets with  $E_T > 20$  GeV,
- (b) Multijet mass  $m > m_{min}$ , and
- (c) the cosine of the leading-jet scattering angle  $\cos \theta < (\cos \theta)_{max}$  where the leading-jet is defined as the highest energy jet in the multijet rest-frame.

Note that for two-jet events the  $\sum E_T$  requirement selects events with jet  $E_T > 210$  GeV. At fixed two-jet mass this results in an effective maximum allowed value of  $\cos\theta$ . The values of  $m_{min}$  and  $(\cos\theta)_{max}$  are chosen to restrict the parameter space to the region in which the  $\sum E_T$  requirement is efficient.

## 2.2 The HERWIG parton shower Monte Carlo calculation

HERWIG [11] is a leading-order QCD parton shower Monte Carlo program that includes both initial- and final-state gluon radiation. HERWIG predictions can be thought of as LO QCD  $2 \rightarrow 2$  predictions with gluon radiation, color coherence, hadronization, and an underlying event. We have used version 5.6 of the HERWIG Monte Carlo program together with a simple detector simulation that modifies the jet energies with a Gaussian resolution function:

$$\sigma_E = 0.1 E . \quad (1)$$

This is similar to the jet energy resolution function reported by the CDF collaboration [1]. In our HERWIG calculations we have used the CTEQ1M [13] structure functions and the scale  $Q^2 = stu/2(s^2+u^2+t^2)$ . HERWIG generates  $2 \rightarrow 2$  processes above a specified  $p_T^{hard}$  where  $p_T^{hard}$  is the  $p_T$  of the outgoing partons from the hard scatter before any radiation has occurred. We have set the minimum  $p_T^{hard}$  to 60 GeV/c. Finally, the HERWIG Monte Carlo distributions discussed in this paper are inclusive. Hence, for a given jet multiplicity  $N$ , the generated events contribute to the distributions if they have at least  $N$  jets that pass the jet requirements. If there are more than  $N$  jets in a generated event, the multijet system is defined using the  $N$  highest  $E_T$  jets.

## 2.3 The NJETS QCD matrix element calculation

The NJETS Monte Carlo program [12] provides parton-level predictions based on the LO QCD  $2 \rightarrow N$  matrix elements. We have used the KMRSD- structure function parameterization's [14] with the renormalization scale chosen to be the average  $p_T$  of the outgoing partons. NJETS does not use a parton fragmentation model. Jet definitions and selection cuts are therefore applied to the final state partons. To enable a direct comparison between NJETS and HERWIG predictions we have smeared the final state parton energies in our NJETS calculations with the jet energy resolution function described above.

In the following we will find that the NJETS and HERWIG predictions are generally in good agreement with one another. This suggests that the QCD predictions for the distributions discussed in this paper are probably not sensitive to reasonable variations in the choice of structure functions,  $Q^2$  scale, jet fragmentation (with the exception of the single-jet mass distributions), or underlying event.

## 2.4 Phase-Space model

We have generated samples of Monte Carlo events for which the multijet systems uniformly populate the N-body phase-space. These phase-space Monte Carlo events were generated with single-jet masses distributed according to the single-jet mass distribution predicted by the HERWIG Monte Carlo program. In addition, the multijet mass distributions were generated according to the corresponding distributions obtained from the HERWIG Monte Carlo calculation. Comparisons between the resulting phase-space model distributions and the corresponding HERWIG and NJETS Monte Carlo distributions help us to understand which multijet parameters are most sensitive to the behaviour of QCD multijet matrix elements.

## 3 Two-Jet Variables

We begin by briefly reviewing the variables that are often used in two-jet analyses [2, 4, 6]. Consider a system of two massless jets. The massless jet approximation is appropriate because at high center-of-mass energies single-jet masses are much smaller than two-jet masses ( $m_{2J}$ ). To describe a system of two massless jets in the two-jet rest-frame we need only two variables. In previous two-jet analyses these variables have often been chosen to be  $m_{2J}$  and  $\cos \theta^*$ , where  $\theta^*$  is the scattering angle between the incoming beam particles and the outgoing jets in the two-jet rest-frame. In defining  $\cos \theta^*$  it must be remembered that in practice a two-jet system will always be produced together with a spectator system, and the incoming beam particles will not be collinear in the two-body rest-frame. Hence, following the convention of Collins and Soper [15]  $\theta^*$  is taken to be the angle between the outgoing jets and the average beam direction. Consider the process  $1 + 2 \rightarrow 3 + 4$ . The center-of-mass scattering angle is defined:

$$\cos \theta^* \equiv \frac{\vec{P}_{AV} \cdot \vec{P}_3}{|\vec{P}_{AV}| |\vec{P}_3|}, \quad (2)$$

where

$$\vec{P}_{AV} = \vec{P}_1 - \vec{P}_2, \quad (3)$$

and we define particle 1 as the incoming interacting parton with the highest energy in the laboratory frame.

NJETS and HERWIG QCD Monte Carlo predictions for the  $m_{2J}$  and  $\cos \theta^*$  distributions are shown in Figs. 1 and 2 respectively for two-jet events produced at the Fermilab Proton-Antiproton Collider satisfying the requirements  $m_{2J} > 550 \text{ GeV}/c^2$  and  $|\cos \theta^*| < 0.6$ . Note that in the HERWIG Monte Carlo calculation the jets acquire mass in the fragmentation process, whereas in the NJETS calculation jets are identified with massless partons. Hence the agreement between the HERWIG and NJETS predictions reflects the validity of the massless jet approximation. The predicted  $\cos \theta^*$  distributions are similar to the angular distribution expected at LO for

$q\bar{q} \rightarrow q\bar{q}$  scattering [16], which is not very different from the well known Rutherford scattering form:

$$\frac{d\sigma}{d\cos\theta^*} \simeq (1 - \cos\theta^*)^{-2}. \quad (4)$$

Hence, the  $\cos\theta^*$  variable has some nice features. Firstly, the LO QCD prediction for the  $\cos\theta^*$  distribution is well known and is similar, although not identical, to the Rutherford scattering distribution. Secondly, the phase-space density is independent of  $\cos\theta^*$ . Therefore the measured  $\cos\theta^*$  distribution depends upon the underlying  $2 \rightarrow 2$  matrix element in a very direct way.

To prepare for the analysis of systems with many jets in the final state it is useful to extend the two-jet variables to describe two-jet systems with massive final state jets. To do this we must specify two additional parameters. Obvious choices are the final state single-jet masses  $m_3$  and  $m_4$ . We prefer to use dimensionless variables, and therefore define:

$$f_3 \equiv \frac{m_3}{m_{2J}}, \quad (5)$$

and

$$f_4 \equiv \frac{m_4}{m_{2J}}, \quad (6)$$

where the jets are ordered in the two-body rest-frame such that  $E_3 > E_4$ , and hence  $f_3 > f_4$ . The HERWIG predictions for the  $f_3$  and  $f_4$  distributions are shown in Fig. 3. Note that  $f_3$  and  $f_4$  are typically of order 0.05 to 0.1, and hence single-jet masses can be neglected for many purposes.

We conclude by noting that we have defined four variables that specify a two-jet system in the two-body rest-frame:  $m_{2J}$ ,  $\cos\theta^*$ ,  $f_3$ , and  $f_4$ .

## 4 Three-Jet Variables

In the standard three-jet analysis used by the UA1 collaboration [3], and later by the CDF [7] and D0 [8] collaborations, five variables are chosen that specify the system of 3 massless particles in the three-body rest-frame. The first of these variables is the three-jet mass ( $m_{3J}$ ). The NJETS and HERWIG predictions for the  $m_{3J}$  distribution are shown in Fig. 4 to be in good agreement with each other. The predicted  $m_{3J}$  distributions have also recently been shown to be in good agreement with the observed CDF  $m_{3J}$  distribution [1]. To complete the description of the three-jet system four additional dimensionless variables are defined that, together with  $m_{3J}$ , span the three-body parameter space. In defining the three-jet parameters it is traditional to label the outgoing jets 3, 4, and 5, and order the jets such that  $E_3 > E_4 > E_5$ , where  $E_j$  is the energy of jet  $j$  in the three-jet rest-frame. The traditional three-jet variables employed are  $X_3$ ,  $X_4$ ,  $\cos\theta_3$ , and  $\psi_3$ , which are defined:

(i)  $X_3$ , the leading-jet energy fraction, normalized:

$$X_3 \equiv \frac{2 E_3}{E_3 + E_4 + E_5} = \frac{2 E_3}{m_{3J}}, \quad (7)$$

(ii)  $X_4$ , the next-to-leading jet energy fraction, normalized:

$$X_4 \equiv \frac{2 E_4}{E_3 + E_4 + E_5} = \frac{2 E_4}{m_{3J}}, \quad (8)$$

(iii)  $\cos \theta_3$ , defined in the three-jet rest-frame as the cosine of the leading-jet scattering angle (see Fig. 5) :

$$\cos \theta_3 \equiv \frac{\vec{P}_{AV} \cdot \vec{P}_3}{|\vec{P}_{AV}| |\vec{P}_3|}. \quad (9)$$

(iv)  $\psi_3$ , defined in the three-jet rest-frame as the angle between the three-jet plane and the plane containing jet 3 (the leading jet) and the average beam direction (see Fig. 5) :

$$\cos \psi_3 \equiv \frac{(\vec{P}_3 \times \vec{P}_{AV}) \cdot (\vec{P}_4 \times \vec{P}_5)}{|\vec{P}_3 \times \vec{P}_{AV}| |\vec{P}_4 \times \vec{P}_5|}. \quad (10)$$

Predictions for the  $X_3$ -,  $X_4$ -,  $\cos \theta_3$ -, and  $\psi_3$ -distributions are shown in Fig. 6 for three-jet events produced at the Fermilab Proton-Antiproton Collider that satisfy the requirements  $m_{3J} > 600 \text{ GeV}/c^2$ ,  $|\cos \theta_3| < 0.6$ , and  $X_3 < 0.9$ . These selection criteria are used to restrict the parameter space to the region for which the  $\sum E_T$  requirement is efficient and to ensure that the jets in the three-jet sample are well measured. The first and second three-jet parameters ( $X_3$  and  $X_4$ ) are Dalitz variables, normalized so that  $X_3 + X_4 + X_5 = 2$ . Momentum conservation restricts the ranges of the Dalitz variables (for massless jets  $2/3 \leq X_3 \leq 1$  and  $1/2 \leq X_4 \leq 1$ ). The phase-space density is uniform over the kinematically allowed region of the  $(X_3, X_4)$ -plane, and hence the phase-space model predictions for the  $X_3$ - and  $X_4$ -distributions can be easily understood. Note that the QCD predictions for the  $X_3$ - and  $X_4$ -distributions are similar to those of the phase-space model. We might have expected the QCD calculations to predict an enhanced event rate as  $X_3 \rightarrow 1$  and the three-jet system therefore approaches a two-jet configuration. However, in practice the algorithm used to define jets and the experimental requirements used to select well measured three-jet events restrict the measured three-jet topologies to those that populate regions of the three-body phase-space where the matrix element varies only slowly over the  $(X_3, X_4)$ -plane. The third and fourth three-jet parameters ( $\cos \theta_3$  and  $\psi_3$ ) are angular variables. The phase-space density is uniform in  $\cos \theta_3$ -space,  $\psi_3$ -space, and is also uniform in the  $(\cos \theta_3, \psi_3)$ -plane. Indeed, the phase-space model does predict a uniform  $\cos \theta_3$  distribution. The phase-space model prediction for the  $\psi_3$  distribution is not quite

uniform, there being a slight depletion of events as  $\psi_3 \rightarrow 0$  or  $\pi$ . This depletion is primarily a consequence of the minimum  $E_T$  requirement used to define jets. We would expect the QCD predictions for the two angular distributions to be very different from the phase-space model predictions. In particular we might expect that the leading-jet angular distribution would be similar, although not identical, to the LO  $q\bar{q} \rightarrow q\bar{q}$  scattering form. Indeed, this is seen to be the case for both the NJETS and HERWIG QCD predictions (Fig. 6c). We might also expect the initial-state radiation pole in the QCD matrix element to result in an enhanced rate of three-jet events for topologies in which the angle between the beam direction and the three-jet plane is small. Hence, we would expect the  $\psi_3$  distribution to be peaked towards 0 and  $\pi$ . This is also evident in the HERWIG and NJETS predictions.

To prepare for the analysis of events with more than three jets we now wish to extend the three-jet variables to describe a system of three massive particles in the three-body rest-frame. To do this we must specify an additional three parameters, which we take to be the single-jet mass fractions  $f_3$ ,  $f_4$ , and  $f_5$  defined:

- (a)  $f_3$ , the leading-jet mass divided by the three-jet mass:

$$f_3 \equiv \frac{m_3}{m_{3J}}, \quad (11)$$

- (b)  $f_4$ , the next-to-leading-jet mass divided by the three-jet mass:

$$f_4 \equiv \frac{m_4}{m_{3J}}, \quad (12)$$

- (c)  $f_5$ , the third-to-leading-jet mass divided by the three-jet mass:

$$f_5 \equiv \frac{m_5}{m_{3J}}. \quad (13)$$

HERWIG predictions for  $f_3$ ,  $f_4$ , and  $f_5$  are shown in Fig. 7. Note that  $f_j$  is typically less than or of order 0.1, and hence single-jet masses can be neglected for many purposes.

We conclude by noting that we have defined eight variables that specify a three-jet system in the three-body rest-frame:  $m_{3J}$ ,  $X_3$ ,  $X_4$ ,  $\cos\theta_3$ ,  $\psi_3$ ,  $f_3$ ,  $f_4$ , and  $f_5$ .

## 5 Four-Jet Variables

To completely describe a system of four jets in the four-body rest-frame we must specify twelve independent parameters. We will choose the four-jet mass ( $m_{4J}$ ) and eleven dimensionless variables that span the four-body parameter space. We have chosen a set of four-jet variables that, for four-jet configurations that approach a three-body topology, reduce to the three-jet variables discussed in the previous section. This will



make it possible to compare the characteristics of four-jet events with the corresponding characteristics of three-jet events.

The four-jet variables are shown schematically in Fig. 8. We begin by reducing the four-jet system to a three-body system by combining the two jets with the lowest two-jet mass. We will label the two jets we combine A and B with  $E_A > E_B$ , where  $E_A$  and  $E_B$  are the jet energies in the four-jet rest-frame. The resulting three-body system can be completely specified using our three-jet variables:  $X_{3'}$ ,  $X_{4'}$ ,  $\cos \theta_{3'}$ ,  $\psi_{3'}$ ,  $f_{3'}$ ,  $f_{4'}$ , and  $f_{5'}$ . Note that we order the three bodies in the three-body rest-frame so that  $E_{3'} > E_{4'} > E_{5'}$ , and use a nomenclature in which primed labels denote objects after two jets have been combined. Hence one of the three primed objects will be the two-jet system (AB). Explicitly,  $X_{3'}$ ,  $X_{4'}$ ,  $\cos \theta_{3'}$ ,  $\psi_{3'}$ ,  $f_{3'}$ ,  $f_{4'}$ , and  $f_{5'}$  are defined:

- (i)  $X_{3'}$ , the fraction of the three-body energy taken by the leading object, normalized:

$$X_{3'} \equiv \frac{2 E_{3'}}{E_{3'} + E_{4'} + E_{5'}} \equiv \frac{2 E_{3'}}{m_{4J}}, \quad (14)$$

- (ii)  $X_{4'}$ , the fraction of the three-body energy taken by the next-to-leading object, normalized:

$$X_{4'} \equiv \frac{2 E_{4'}}{E_{3'} + E_{4'} + E_{5'}} \equiv \frac{2 E_{4'}}{m_{4J}}, \quad (15)$$

- (iii)  $\cos \theta_{3'}$ , the cosine of the leading-body scattering angle:

$$\cos \theta_{3'} \equiv \frac{\vec{P}_{AV} \cdot \vec{P}_{3'}}{|\vec{P}_{AV}| |\vec{P}_{3'}|}, \quad (16)$$

- (iv)  $\psi_{3'}$ , the angle between the three-body plane and the plane containing object 3' (the leading body) and the average beam direction:

$$\cos \psi_{3'} \equiv \frac{(\vec{P}_{3'} \times \vec{P}_{AV}) \cdot (\vec{P}_{4'} \times \vec{P}_{5'})}{|\vec{P}_{3'} \times \vec{P}_{AV}| |\vec{P}_{4'} \times \vec{P}_{5'}|}, \quad (17)$$

- (v)  $f_{3'}$ , the mass of the leading object divided by the four-jet mass:

$$f_{3'} \equiv \frac{m_{3'}}{m_{4J}}, \quad (18)$$

- (vi)  $f_{4'}$ , the mass of the next-to-leading object divided by the four-jet mass:

$$f_{4'} \equiv \frac{m_{4'}}{m_{4J}}, \quad (19)$$

- (vii)  $f_{5'}$ , the mass of the third-to-leading object divided by the four-jet mass:

$$f_{5'} \equiv \frac{m_{5'}}{m_{4J}}. \quad (20)$$

The NJETS and HERWIG predictions for the  $m_{4J}$  distribution are shown in Fig. 9 for four-jet events produced at the Fermilab Proton-Antiproton Collider satisfying the requirements  $m_{4J} > 650 \text{ GeV}/c^2$ ,  $|\cos \theta_{3'}| < 0.8$ , and  $X_{3'} < 0.9$ . The QCD predictions for the  $X_{3'}$ -,  $X_{4'}$ -,  $\cos \theta_{3'}$ -, and  $\psi_{3'}$ -distributions are compared with the phase-space model predictions in Fig. 10. There is reasonable agreement between the HERWIG and NJETS predictions for all of these distributions. The QCD predictions for the  $X_{3'}$ - and  $X_{4'}$ -distributions are not very different from the predictions of the phase-space model. In contrast, the NJETS and HERWIG  $\cos \theta_{3'}$ - and  $\psi_{3'}$ -distributions are very different from the more uniform phase-space model predictions. It is interesting to compare these distributions with the equivalent distributions for three-jet events (Fig. 6). The QCD and phase-space model predictions for the four-jet distributions are similar but not identical to the corresponding distributions for three-jet events. Note that (1) in comparing the phase-space model predictions for the  $X_{3'}$ - and  $X_{3'}$ -distributions we see that the predicted  $X_{3'}$  distribution is depleted at large  $X_{3'}$ , and (2) in comparing the phase-space model predictions for the  $X_{4'}$ - and  $X_{4'}$ -distributions we see that the predicted  $X_{4'}$  distribution is distorted at large  $X_{4'}$ . These differences can be qualitatively understood by noting that if  $4'$  or  $5'$  is the (AB)-system and hence massive then  $X_{3'} < 1$  even if  $4'$  and  $5'$  are collinear. It should also be noted that the phase-space model  $\cos \theta_{3'}$  distribution is slightly depleted at small  $|\cos \theta_{3'}|$  and the  $\psi_{3'}$  distribution is slightly depleted for values of  $\psi_{3'}$  close to 0 and  $\pi$ . These features are consequences of the minimum jet-jet separation requirement  $\Delta R > 0.9$ , and the minimum jet transverse energy requirement  $E_T > 20 \text{ GeV}$ .

The HERWIG predictions for the normalized single-jet masses  $f_{j'}$  are shown in Fig. 11. They exhibit peaks close to  $f_{j'} = 0.05$  which reflect the finite single-jet masses resulting from the HERWIG fragmentation model, and long tails at larger values of  $f_{j'}$  which reflect the contributions from the combined (AB)-systems. Note that although single jets are massless in the NJETS calculation, the NJETS program does predict the contribution to the  $f_{j'}$ -distributions from the combined (AB)-systems, and indeed the NJETS and HERWIG predictions are in good agreement at large  $f_{j'}$ .

To complete our description of the four-jet system we must now specify four additional parameters that describe the two-jet (AB)-system. To describe the (AB)-system we choose:

- (a)  $f_A$ , the mass of jet A divided by the four-jet mass:

$$f_A \equiv \frac{m_A}{m_{4J}}, \quad (21)$$

- (b)  $f_B$ , the mass of jet B divided by the four-jet mass:

$$f_B \equiv \frac{m_B}{m_{4J}}, \quad (22)$$

- (c)  $X_A$ , defined in the four-jet rest-frame as the fraction of the energy of the (AB)-system taken by the leading jet:

$$X_A \equiv \frac{E_A}{E_A + E_B}, \quad (23)$$

- (d)  $\psi'_{AB}$ , defined in the four-jet rest-frame as the angle between (i) the plane containing the (AB)-system and the average beam direction, and (ii) the plane containing A and B (see Fig. 8). The prime reminds us that in order to define  $\psi'_{AB}$  we have combined two jets to obtain the (AB)-system. Note that:

$$\cos \psi'_{AB} \equiv \frac{(\vec{P}_A \times \vec{P}_B) \cdot (\vec{P}_{AB} \times \vec{P}_{AV})}{|\vec{P}_A \times \vec{P}_B| |\vec{P}_{AB} \times \vec{P}_{AV}|}. \quad (24)$$

The predicted  $f_{A-}$  and  $f_{B-}$  distributions are shown in Figs. 12 (a) and 12 (b) respectively. The typical values of  $f_A$  and  $f_B$  predicted by the HERWIG fragmentation model are less than or of order 0.05. The predicted  $X_A$  distributions are shown in Fig. 12 (c). The NJETS and HERWIG QCD calculations yield harder  $X_A$  distributions than the corresponding distribution predicted by the phase-space model. Presumably this reflects the presence of the soft gluon radiation pole in the QCD matrix element. To gain some insight into the shape of the phase-space model prediction for the  $X_A$  distribution consider a system of four massless particles labelled randomly i, j, k, and l. If we define  $X_i \equiv E_i/(E_i + E_j)$ , then the phase-space prediction for the distribution of events as a function of  $X_i$  is given by:

$$\frac{dN}{dX_i} \sim \frac{3}{X_i^2} - \frac{1}{X_i^3} - 2. \quad (25)$$

This function is already quite similar to the phase-space model prediction shown in Fig. 12 (c), which is obtained by requiring that the (AB)-system is the lowest mass pair, and taking account of finite single-jet masses and experimental selection requirements. Finally, the predicted  $\psi'_{AB}$  distributions are shown in Fig. 12 (d). The NJETS and HERWIG predictions for the  $\psi'_{AB}$  distribution are in agreement with one another. The slight decrease in the population of events predicted by the phase-space model as  $\psi'_{AB}$  approaches 0 or  $\pi$  is a consequence of the minimum jet  $E_T$  requirement.

We conclude by noting that we have defined twelve variables that specify a four-jet system in the four-body rest-frame:  $m_{4J}$ ,  $X_{3'}$ ,  $X_{4'}$ ,  $\cos \theta_{3'}$ ,  $\psi_{3'}$ ,  $f_{3'}$ ,  $f_{4'}$ ,  $f_{5'}$ ,  $f_A$ ,  $f_B$ ,  $X_A$ , and  $\psi'_{AB}$ .

## 6 Five-Jet Variables

To completely describe a system of five jets in the five-body rest-frame we must specify sixteen independent parameters. We will choose the five-jet mass ( $m_{5J}$ ) and fifteen

dimensionless variables that span the five-body parameter space. We have chosen a set of five-jet variables that, for five-body configurations that approach a four-body topology, reduce to the four-jet variables discussed in the previous section. Furthermore, for five-body configurations that approach a three-body topology, our five-jet parameters reduce to the three-jet variables discussed previously. Thus we will be able to compare the characteristics of five-jet events with the corresponding characteristics of three-jet and four-jet events.

The five-jet variables are shown schematically in Fig. 13. We begin by reducing the five-jet system to a four-body system by combining the two jets with the lowest two-jet mass. We will label the two jets we combine C and D, with  $E_C > E_D$ , where  $E_C$  and  $E_D$  are the jet energies in the five-jet rest-frame. We can then further reduce the resulting four-body system to a three-body system by combining the two bodies with the lowest two-body mass. We will label the two objects we combine  $A'$  and  $B'$ , with  $E_{A'} > E_{B'}$ . The resulting three-body system can be completely specified using our three-jet variables:  $X_{3''}$ ,  $X_{4''}$ ,  $\cos \theta_{3''}$ ,  $\psi_{3''}$ ,  $f_{3''}$ ,  $f_{4''}$ , and  $f_{5''}$ . Note that we order the three bodies such that  $E_{3''} > E_{4''} > E_{5''}$ , and use a nomenclature in which doubly primed labels denote objects after two operations in which the two bodies with the lowest two-body mass have been combined. One of the three doubly primed objects will be the  $(A'B')$ -system. Explicitly,  $X_{3''}$ ,  $X_{4''}$ ,  $\cos \theta_{3''}$ ,  $\psi_{3''}$ ,  $f_{3''}$ ,  $f_{4''}$ , and  $f_{5''}$  are defined:

- (i)  $X_{3''}$ , the fraction of the three-body energy taken by the leading body, normalized:

$$X_{3''} \equiv \frac{2 E_{3''}}{E_{3''} + E_{4''} + E_{5''}} = \frac{2E_{3''}}{m_{5J}}, \quad (26)$$

- (ii)  $X_{4''}$ , the fraction of the three-body energy taken by the next-to-leading body, normalized:

$$X_{4''} \equiv \frac{2 E_{4''}}{E_{3''} + E_{4''} + E_{5''}} = \frac{2E_{4''}}{m_{5J}}, \quad (27)$$

- (iii)  $\cos \theta_{3''}$ , the cosine of the leading-body scattering angle:

$$\cos \theta_{3''} \equiv \frac{\vec{P}_{AV} \cdot \vec{P}_{3''}}{|\vec{P}_{AV}| |\vec{P}_{3''}|}, \quad (28)$$

- (iv)  $\psi_{3''}$ , the angle between the three-body plane and the plane containing object 3'' (the leading body) and the average beam direction:

$$\cos \psi_{3''} \equiv \frac{(\vec{P}_{3''} \times \vec{P}_{AV}) \cdot (\vec{P}_{4''} \times \vec{P}_{5''})}{|\vec{P}_{3''} \times \vec{P}_{AV}| |\vec{P}_{4''} \times \vec{P}_{5''}|}, \quad (29)$$

- (v)  $f_{3''}$ , the normalized mass of the leading object:

$$f_{3''} \equiv \frac{m_{3''}}{m_{5J}}, \quad (30)$$

(vi)  $f_{4''}$ , the normalized mass of the next-to-leading object:

$$f_{4''} \equiv \frac{m_{4''}}{m_{5J}} , \quad (31)$$

(vii)  $f_{5''}$ , the normalized mass of the third-to-leading object:

$$f_{5''} \equiv \frac{m_{5''}}{m_{5J}} . \quad (32)$$

The NJETS and HERWIG predictions for the  $m_{5J}$  distribution are shown in Fig. 14 for five-jet events produced at the Fermilab Proton-Antiproton Collider and satisfying the requirement  $m_{5J} > 750 \text{ GeV}/c^2$ . The QCD predictions for the  $X_{3''-}$ ,  $X_{4''-}$ ,  $\cos \theta_{3''-}$ , and  $\psi_{3''-}$ -distributions are compared with the phase-space model predictions in Fig. 15. The predicted distributions are qualitatively similar to the equivalent four-jet distributions shown in Fig. 10. Note that the QCD predictions for the  $\cos \theta_{3''}$  distribution are remarkably similar to the simple LO  $q\bar{q} \rightarrow q\bar{q}$  angular distribution.

The HERWIG predictions for the normalized single-jet masses  $f_{j''}$  are shown in Fig. 16. Once again, the HERWIG and NJETS distributions are in agreement at large mass fractions.

We must now specify the intermediate four-body system. In analogy with the four-jet analysis we will do this by specifying four additional dimensionless variables that describe the  $(A'B')$ -system. We choose  $f_{A'}$ ,  $f_{B'}$ ,  $X_{A'}$ , and  $\psi''_{A'B'}$ , defined:

(a)  $f_{A'}$ , the normalized mass of object  $A'$ :

$$f_{A'} \equiv \frac{m_{A'}}{m_{5J}} , \quad (33)$$

(b)  $f_{B'}$ , the normalized mass of object  $B'$ :

$$f_{B'} \equiv \frac{m_{B'}}{m_{5J}} , \quad (34)$$

(c)  $X_{A'}$ , defined in the five-jet rest-frame as the fraction of the energy of the  $(A'B')$ -system taken by the leading body:

$$X_{A'} \equiv \frac{E_{A'}}{E_{A'} + E_{B'}} , \quad (35)$$

(d)  $\psi''_{A'B'}$ , defined in the five-jet rest-frame as the angle between (i) the plane containing the  $(A'B')$ -system and the average beam direction, and (ii) the plane containing  $A'$  and  $B'$  (see Fig. 13). Note that:

$$\cos \psi''_{A'B'} \equiv \frac{(\vec{P}_{A'} \times \vec{P}_{B'}) \cdot (\vec{P}_{A'B'} \times \vec{P}_{AV})}{|\vec{P}_{A'} \times \vec{P}_{B'}| |\vec{P}_{A'B'} \times \vec{P}_{AV}|} . \quad (36)$$

The predicted distributions of these variables are shown in Fig. 17. The HERWIG predictions for the  $f_{A'}$ - and  $f_{B'}$ -distributions peak at values of about 0.02 and have long tails associated with composite  $A'$  or  $B'$  systems. The tails are accounted for by the NJETS predictions. It is interesting to compare the  $X_{A'}$ - and  $\psi''_{A'B'}$ -distributions with the corresponding four-jet distributions (Figs. 12 (c) and 12 (d) respectively). The QCD and phase-space model predictions for the five-jet distributions are qualitatively similar to the corresponding four-jet distributions. Note that the HERWIG and NJETS predictions are in agreement with one another.

Finally, to complete our specification of the five-jet system we must define a further four variables that describe the two-body (CD)-system. We choose  $f_C$ ,  $f_D$ ,  $X_C$ , and  $\psi''_{CD}$ , defined:

- (a)  $f_C$ , the normalized mass of jet C:

$$f_C \equiv \frac{m_C}{m_{5J}}, \quad (37)$$

- (b)  $f_D$ , the normalized mass of jet D:

$$f_D \equiv \frac{m_D}{m_{5J}}, \quad (38)$$

- (c)  $X_C$ , defined in the five-jet rest-frame as the fraction of the energy of the (CD)-system taken by the leading jet:

$$X_C \equiv \frac{E_C}{E_C + E_D}, \quad (39)$$

- (d)  $\psi''_{CD}$ , defined in the five-jet rest-frame as the angle between (i) the plane containing the (CD)-system and the average beam direction and (ii) the plane containing C and D (see Fig. 13). Note that:

$$\cos \psi''_{CD} \equiv \frac{(\vec{P}_C \times \vec{P}_D) \cdot (\vec{P}_{CD} \times \vec{P}_{AV})}{|\vec{P}_C \times \vec{P}_D| |\vec{P}_{CD} \times \vec{P}_{AV}|}. \quad (40)$$

The predicted distributions of these variables are shown in Fig. 18. The HERWIG predictions for the  $f_{A'}$ - and  $f_{B'}$ -distributions peak at values less than 0.02. Note that the QCD predictions for the  $X_C$  distribution are harder than the corresponding phase-space model prediction, whilst the QCD predictions for the  $\psi''_{CD}$ -distribution are similar to the corresponding phase-space model prediction.

We conclude by noting that we have defined sixteen variables that specify a five-jet system in the five-body rest-frame:  $m_{5J}$ ,  $X_{3''}$ ,  $X_{4''}$ ,  $\cos \theta_{3''}$ ,  $\psi_{3''}$ ,  $f_{3''}$ ,  $f_{4''}$ ,  $f_{5''}$ ,  $f_{A'}$ ,  $f_{B'}$ ,  $X_{A'}$ ,  $\psi''_{A'B'}$ ,  $f_C$ ,  $f_D$ ,  $X_C$ , and  $\psi''_{CD}$ .

## 7 Generalization to Events with Six or More Jets

A list of the multijet variables described in the preceding sections is given in Table 1. The extension of the variables to describe multijet systems with more than five jets is straight forward. As an example the variables required to describe a six-jet event are also listed in Table 1. In general, to describe an event containing  $N$  jets we use the mass of the  $N$ -jet system plus  $(4N-5)$  dimensionless variables. To define the dimensionless variables we proceed by reducing the  $N$ -jet system to a three-body system. This is done in  $(N-3)$  steps. In each step the two bodies with the lowest two-body mass are combined by adding the two four-vectors. The resulting three-body system is described by specifying seven parameters, namely the normalized masses of the three bodies (e.g.  $f_3$ ,  $f_4$ , and  $f_5$ ), the Dalitz variables for the two leading bodies (e.g.  $X_3$  and  $X_4$ ), the cosine of the leading-body scattering angle (e.g.  $\cos\theta_3$ ), and the angle between the three-body plane and the beam direction (e.g.  $\psi_3$ ). To complete the description of the  $N$ -jet system we must then specify an additional four parameters for each step in which two bodies were combined. These parameters are the normalized masses of the two bodies (e.g.  $f_A$  and  $f_B$ ), the fraction of the two-body energy taken by the leading body (e.g.  $X_A$ ), and the angle defined in the  $N$ -jet rest-frame between the plane containing the two-body system and the beam direction and the plane defined by the two bodies (e.g.  $\psi'_{AB}$ ).

## 8 Summary

We have defined a set of  $(4N - 4)$  parameters that can be used to analyse events in which  $N$  jets have been produced in high energy hadron-hadron collisions. These multijet parameters (i) span the multijet parameter space, (ii) facilitate the interpretation of observed event distributions within the framework of perturbative QCD, and (iii) make it possible to compare the characteristics of events having  $N$  jets with the characteristics of events having for example  $(N+1)$  jets.

To illustrate the use of the multijet variables described in this paper we have discussed QCD and phase-space model predictions for three-jet, four-jet, and five-jet events produced at the Fermilab Proton-Antiproton Collider. For this particular example we note that, apart from small effects that can be ascribed to the absence of a fragmentation model in the NJETS calculation, the complete LO QCD matrix element predictions for each of the multijet parameter distributions discussed in the preceding sections are well described by the parton shower Monte Carlo calculation. Thus it appears that even when there are five hard partons in the final state a good approximation to the LO QCD matrix element is given by  $2 \rightarrow 2$  scattering plus gluon radiation. This is of interest because the complete LO matrix element calculation is not at present available for topologies with more than five final state partons. Hence for the analysis of events with six or more jets we must rely on parton shower Monte Carlo calculations, or on other approximations to the QCD matrix element.

Finally, the multijet variables discussed in this paper have been selected to emphasize simple to interpret quantities (masses, energy fractions, scattering angles, and planarity-type angles). Wherever possible we have tried to select parameters for which the phase-space model distributions are simple to understand. Experimental requirements used to select well measured N-jet events necessarily distort some of the predicted distributions. However, for the example discussed in this paper, we note that for most parameters the experimental selection criteria result in modifications to the phase-space model predictions that are modest and are limited to small regions of the parameter space. The observed N-jet distributions should therefore directly reflect the dynamics of the underlying multijet matrix element.

We are grateful to Walter Giele for many interesting discussions. This work was supported by the U.S. Department of Energy, and the Ministry of Science, Culture and Education of Japan.



## References

- [1] F. Abe et al. (CDF Collaboration), *Phys. Rev. Lett.* **75**, 608 (1995).
- [2] G. Arnison et al. (UA1 Collaboration), *Phys. Lett.* **123B**, 115 (1983); **132B**, 214 (1983); **136B**, 294 (1984); **177B**, 244 (1986); C. Albajar et al. (UA1 Collaboration), *Phys. Lett.* **209B**, 127 (1988).
- [3] G. Arnison et al. (UA1 Collaboration), *Phys. Lett.* **158B**, 494 (1985).
- [4] M. Banner et al. (UA2 Collaboration), *Phys. Lett.* **118B**, 203 (1982); P. Bagnaia et al. (UA2 Collaboration), *Phys. Lett.* **138B**, 430 (1984); **144B**, 283 (1984); J. A. Appel et al. (UA2 Collaboration), *Phys. Lett.* **165B**, 441 (1985); J. Alitti et al. (UA2 Collaboration), *Z. Phys.* **C49**, 17 (1991).
- [5] J. A. Appel et al. (UA2 Collaboration), *Z. Phys.* **C30**, 341 (1986).
- [6] F. Abe et al. (CDF Collaboration), *Phys. Rev. Lett.* **62**, 3020 (1989); **64**, 157 (1990); **69**, 2896 (1992); **71**, 2542 (1993); *Phys. Rev.* **D41**, 1722 (1990); **D48**, 998 (1993).
- [7] F. Abe et al. (CDF Collaboration), *Phys. Rev.* **D45**, 1448 (1992).
- [8] S. Abachi et al. (D0 Collaboration), *FERMILAB Conf-95/214-E* submitted to the Int. Conf. on High Energy Physics, Brussels, Belgium, July 27 - Aug. 2 (1995).
- [9] J. Alitti et al. (UA2 Collaboration), *Phys. Lett.* **268B**, 145 (1991).
- [10] F. Abe et al. (CDF Collaboration), *Phys. Rev.* **D47**, 4857 (1993).
- [11] G. Marchesini and B. Webber, *Nucl. Phys.* **B310**, 461 (1988).
- [12] F.A. Berends, W. Giele, and H. Kuijf, *Nucl. Phys.* **B333**, 120 (1990); *Phys. Lett.* **232B**, 266 (1990); F.A. Berends and H. Kuijf, *Nucl. Phys.* **B353**, 59 (1991).
- [13] H.L. Lai et al; Preprint MSU-HEP-41024, CTEQ-404, (to be published).
- [14] A.D. Martin, R.G. Roberts, W.J. Stirling; *Phys. Lett.* **B306**, 145 (1993).
- [15] J. Collins and D. Soper, *Phys. Rev.* **D16**, 2219 (1977).
- [16] B. L. Combridge and C. J. Maxwell, *Nucl. Phys.* **B239**, 429 (1984).

Two-Jet	Three-Jet	Four-Jet	Five-Jet	Six-Jet
$m_{2J}$	$m_{3J}$	$m_{4J}$	$m_{5J}$	$m_{6J}$
$\cos \theta^\star$	$\cos \theta_3$	$\cos \theta_{3'}$	$\cos \theta_{3''}$	$\cos \theta_{3'''}$
$f_3$	$f_3$	$f_{3'}$	$f_{3''}$	$f_{3'''}$
$f_4$	$f_4$	$f_{4'}$	$f_{4''}$	$f_{4'''}$
	$f_5$	$f_{5'}$	$f_{5''}$	$f_{5'''}$
	$\psi_3$	$\psi_{3'}$	$\psi_{3''}$	$\psi_{3'''}$
	$X_3$	$X_{3'}$	$X_{3''}$	$X_{3'''}$
	$X_4$	$X_{4'}$	$X_{4''}$	$X_{4'''}$
		$f_A$	$f_{A'}$	$f_{A''}$
		$f_B$	$f_{B'}$	$f_{B''}$
		$X_A$	$X_{A'}$	$X_{A''}$
		$\psi'_{AB}$	$\psi''_{A'B'}$	$\psi'''_{A''B''}$
			$f_C$	$f_{C'}$
			$f_D$	$f_{D'}$
			$X_C$	$X_{C'}$
			$\psi''_{CD}$	$\psi'''_{C'D'}$
				$f_E$
				$f_F$
				$X_E$
				$\psi'''_{EF}$

Table 1: Summary of the (4N-4) multijet variables for N = 2, 3, 4, 5, and 6.

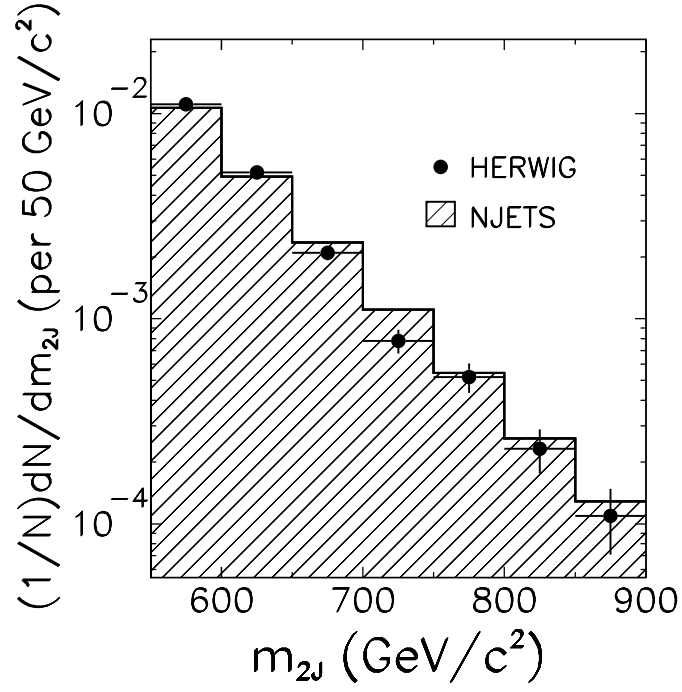


Figure 1: Predicted two-jet mass distributions for two-jet events produced at the Fermilab Proton-Antiproton Collider. HERWIG (points) compared with NJETS (histogram) after applying the requirements of  $m_{2J} > 550 \text{ GeV}/c^2$  and  $|\cos \theta^*| < 0.6$ .

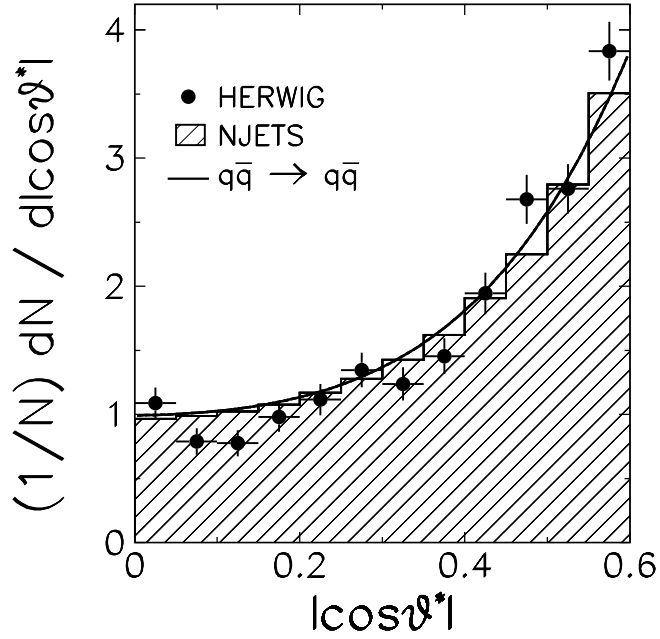


Figure 2: Predicted  $|\cos \theta^*|$  distributions for two-jet events produced at the Fermilab Proton-Antiproton Collider that satisfy the requirements  $m_{2J} > 550 \text{ GeV}/c^2$  and  $|\cos \theta^*| < 0.6$ . The HERWIG prediction (points) is compared with the NJETS prediction (histogram), and the LO QCD prediction for  $q\bar{q} \rightarrow q\bar{q}$  scattering (curve).

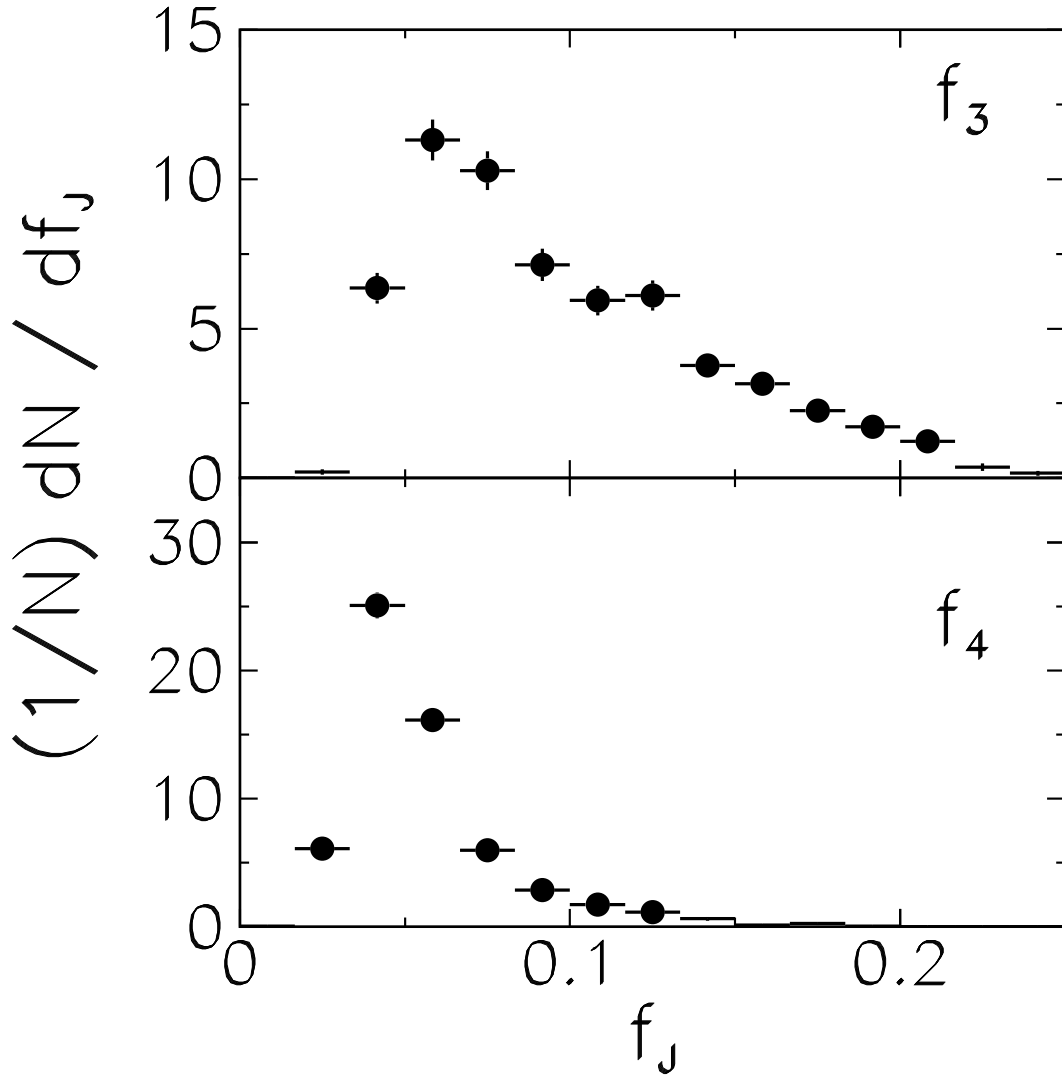


Figure 3: The HERWIG Monte Carlo predictions for the distributions of leading and next-to-leading single-jet-mass fractions for jets in two-jet events produced at the Fermilab Proton-Antiproton Collider that satisfy the requirements  $m_{2J} > 550 \text{ GeV}/c^2$  and  $|\cos \theta^*| < 0.6$ .

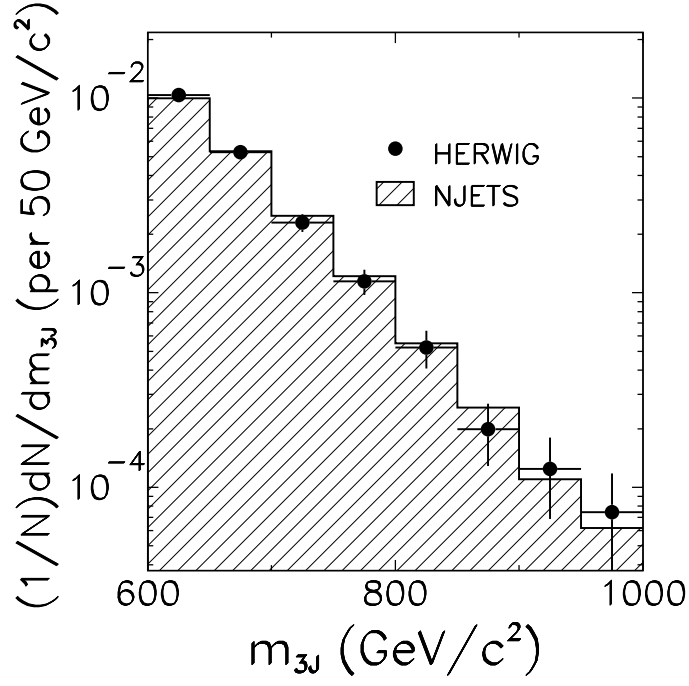


Figure 4: Predicted three-jet mass distributions for events produced at the Fermilab Proton-Antiproton Collider that satisfy the requirements  $m_{3J} > 600 \text{ GeV}/c^2$ ,  $X_3 < 0.9$ , and  $|\cos\theta_3| < 0.6$ . HERWIG predictions (points) are compared with NJETS predictions (histogram).

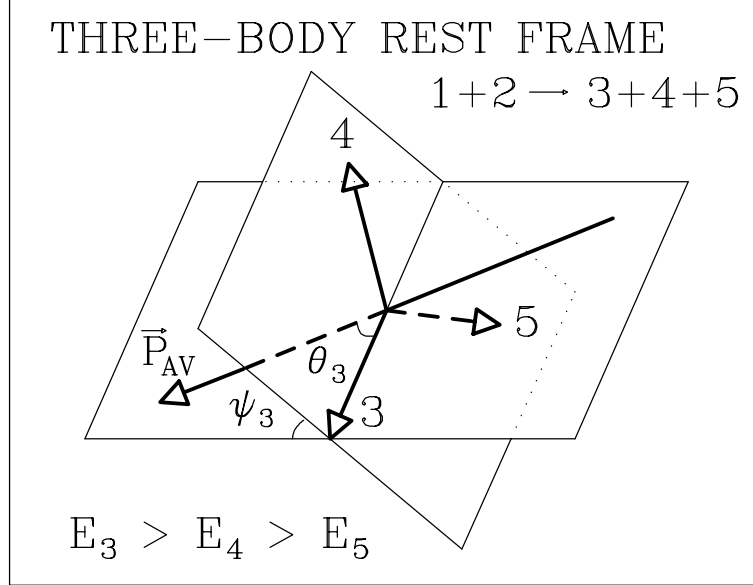


Figure 5: Schematic definition of angles used to describe the three-jet system in the three-jet rest-frame.

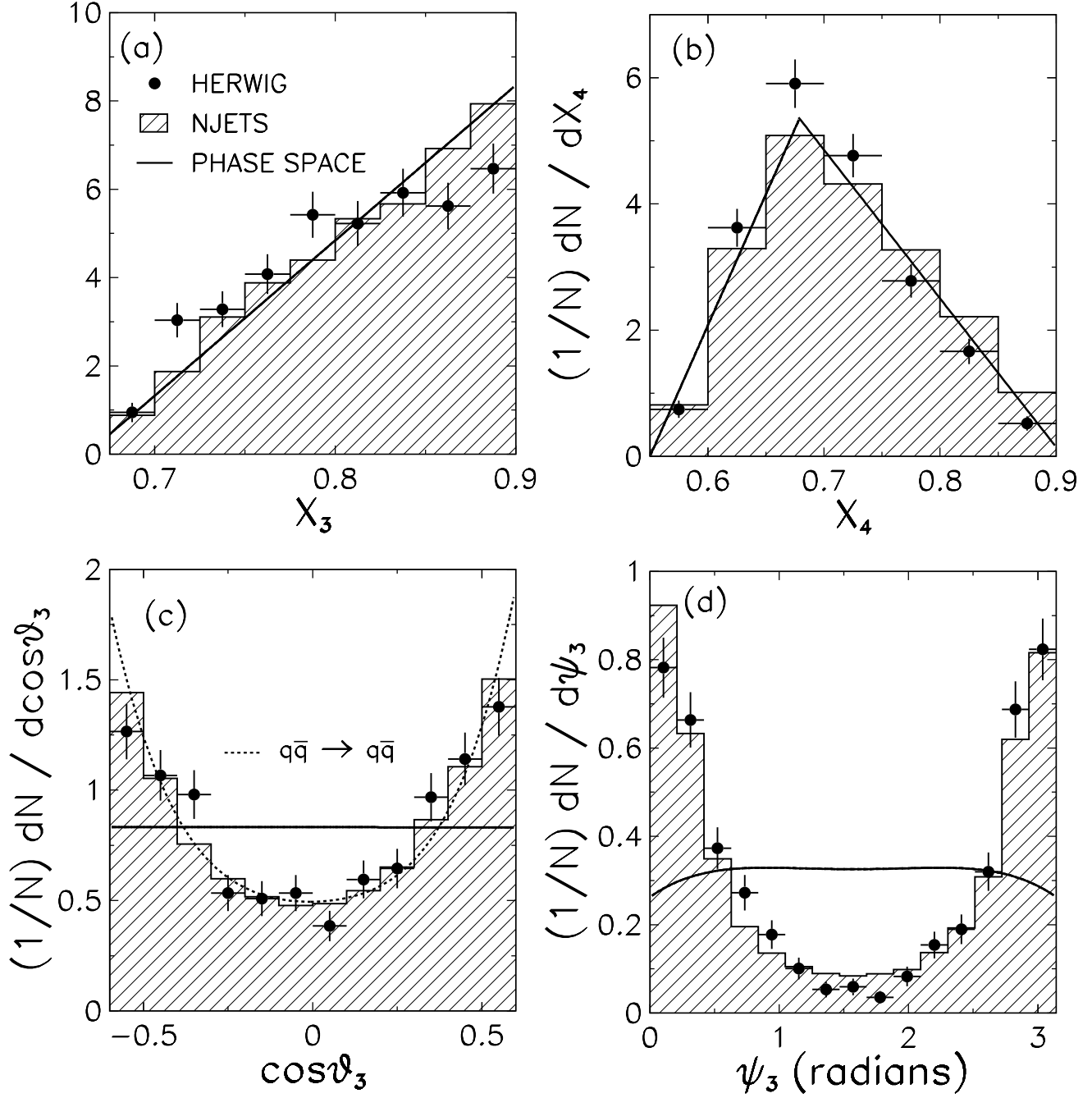


Figure 6: Predicted distributions of the three-jet variables defined in the text for three-jet events produced at the Fermilab Proton-Antiproton Collider that satisfy the requirements  $m_{3J} > 600 \text{ GeV}/c^2$ ,  $X_3 < 0.9$ , and  $|\cos \theta_3| < 0.6$ . HERWIG predictions (points) are compared with NJETS predictions (histograms) and the phase-space model predictions (solid curves) for (a)  $X_3$ , (b)  $X_4$ , (c)  $\cos \theta_3$ , and (d)  $\psi_3$ . The broken curve in the  $\cos \theta_3$  figure is the LO QCD prediction for  $q\bar{q} \rightarrow q\bar{q}$  scattering.

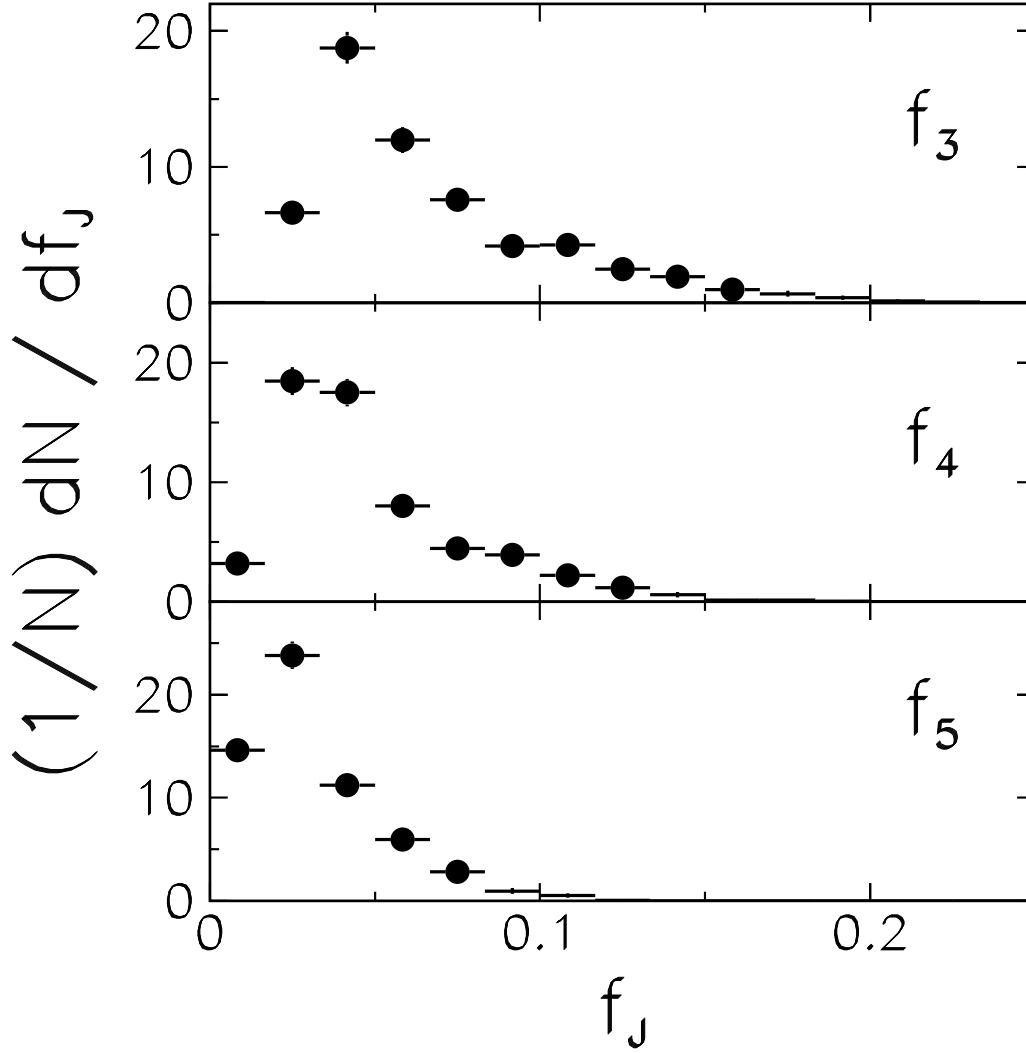


Figure 7: HERWIG Monte Carlo predictions for the single-jet mass-fraction distributions for jets in three-jet events produced at the Fermilab Proton-Antiproton Collider that satisfy the requirements  $m_{3J} > 600 \text{ GeV}/c^2$ ,  $X_3 < 0.9$ , and  $|\cos \theta_3| < 0.6$ .

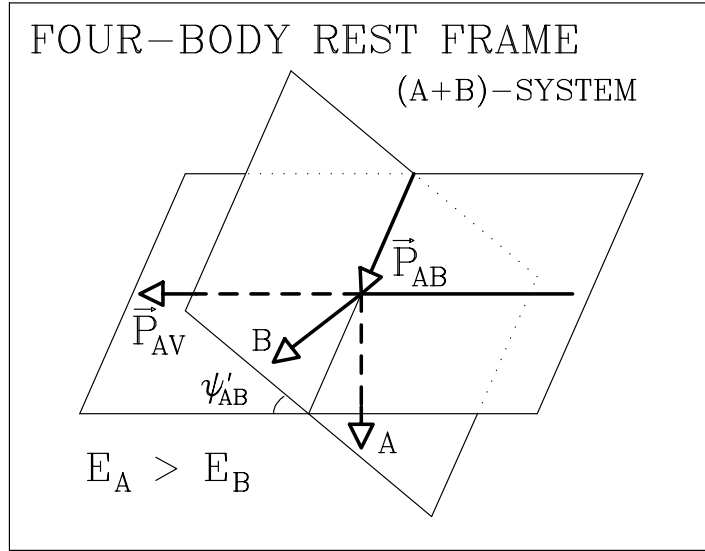
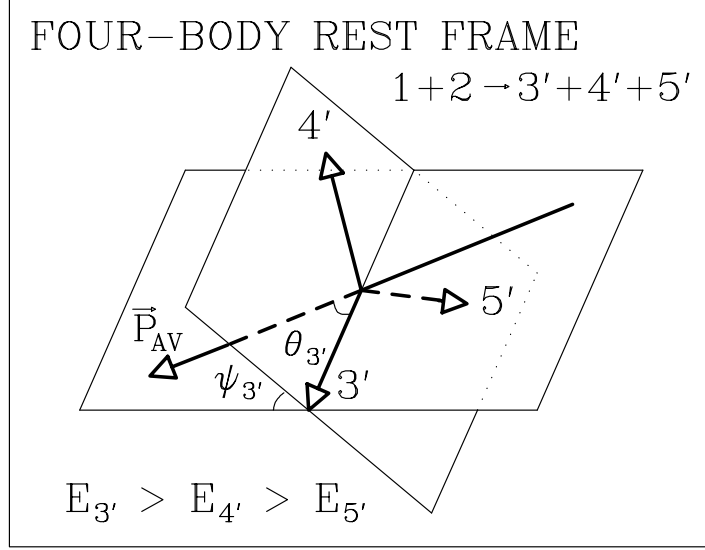


Figure 8: Schematic definition of angles used to describe the four-jet system in the four-jet rest-frame.



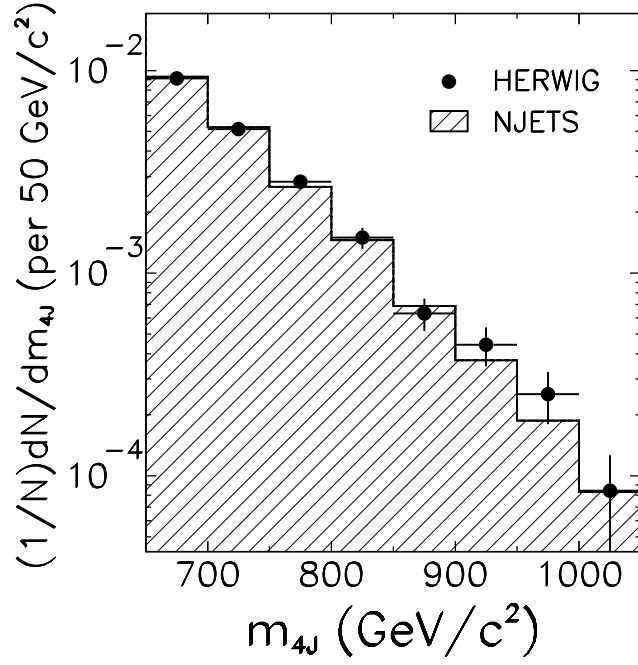


Figure 9: Predicted four-jet mass distributions for events produced at the Fermilab Proton-Antiproton Collider that satisfy the requirements  $m_{4J} > 650 \text{ GeV}/c^2$ ,  $X_{3'} < 0.9$ , and  $|\cos \theta_{3'}| < 0.8$ . HERWIG predictions (points) are compared with NJETS predictions (histogram).

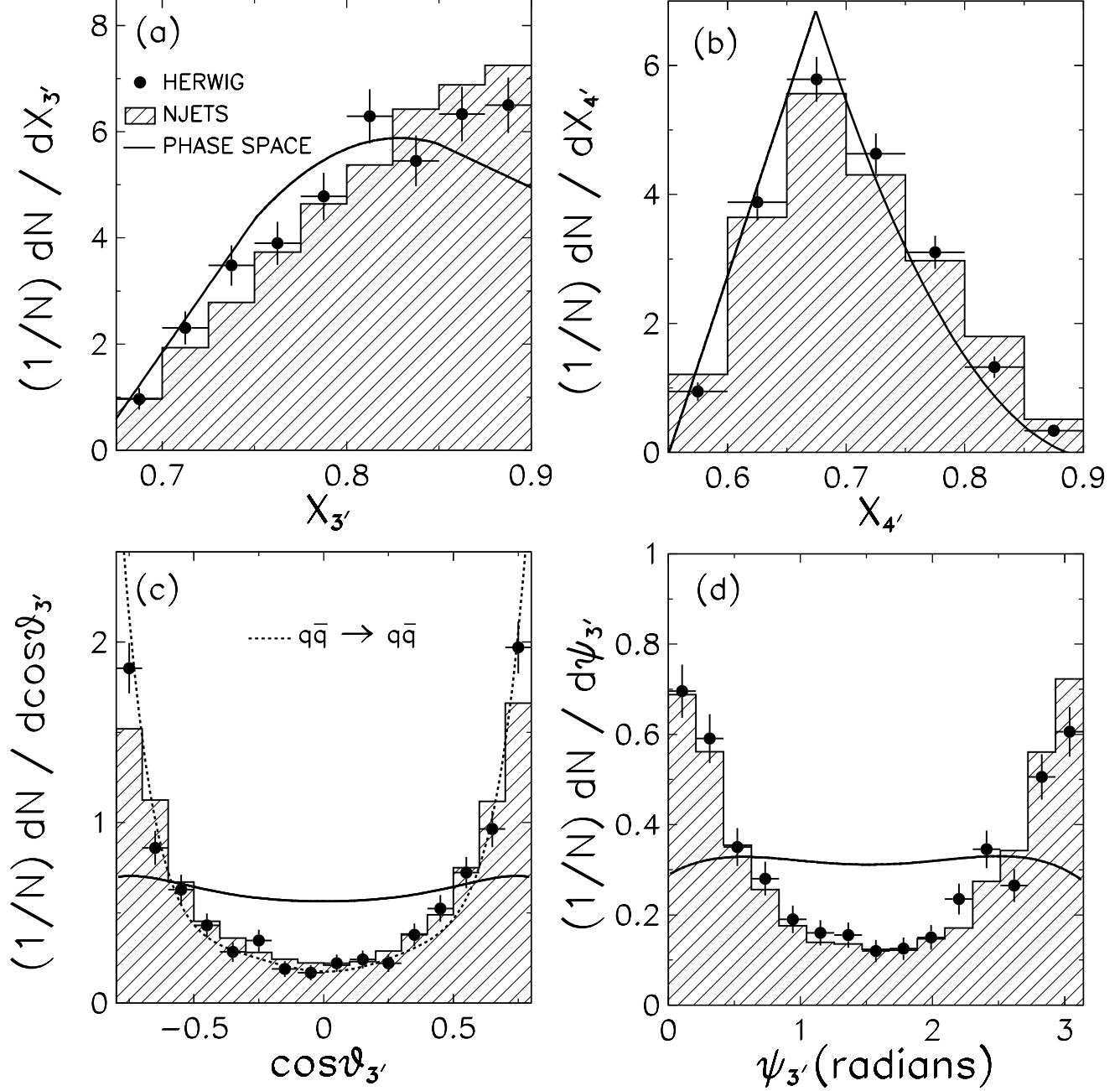


Figure 10: Predicted distributions of three-body variables described in the text for four-jet events produced at the Fermilab Proton-Antiproton Collider that satisfy the requirements  $m_{4J} > 650 \text{ GeV}/c^2$ ,  $X_{3'} < 0.9$ , and  $|\cos\theta_{3'}| < 0.8$ . The HERWIG predictions (points) are compared with NJETS predictions (histograms), and with the phase-space model predictions (solid curves) for (a)  $X_{3'}$ , (b)  $X_{4'}$ , (c)  $\cos\theta_{3'}$ , and (d)  $\psi_{3'}$ . The broken curve in the  $\cos\theta_{3'}$  figure is the LO QCD prediction for  $q\bar{q} \rightarrow q\bar{q}$  scattering.

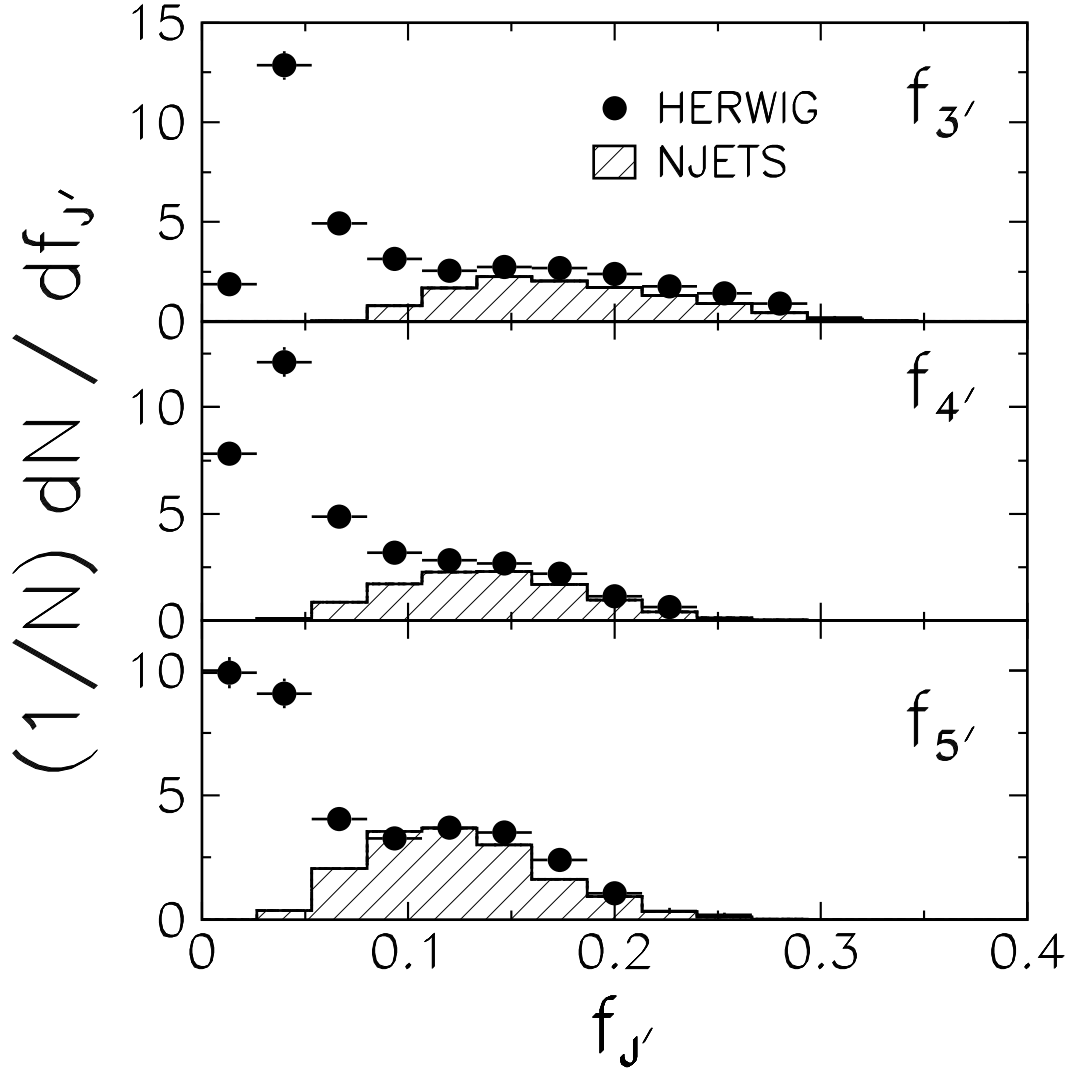


Figure 11: The predicted distributions of single-jet mass-fractions for jets in four-jet events produced at the Fermilab Proton-Antiproton Collider that satisfy the requirements  $m_{4J} > 650 \text{ GeV}/c^2$ ,  $X_{3'} < 0.9$ , and  $|\cos \theta_{3'}| < 0.8$ . HERWIG predictions (points) are compared with NJETS predictions (histograms).

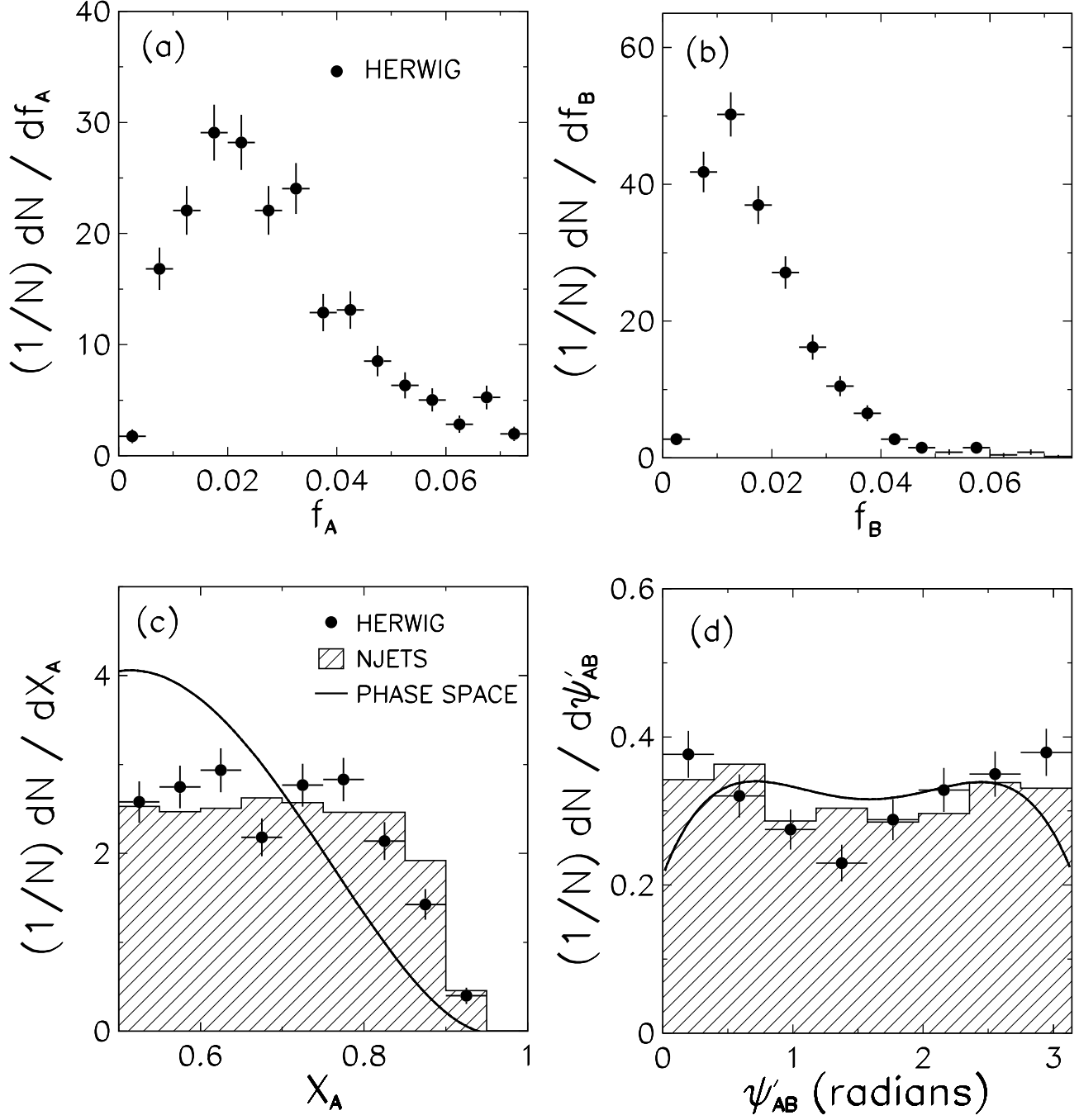


Figure 12: The predicted distributions of the four-jet variables describing the (AB)-system for four-jet events produced at the Fermilab Proton-Antiproton Collider that satisfy the requirements  $m_{4J} > 650 \text{ GeV}/c^2$ ,  $X_{3'} < 0.9$ , and  $|\cos \theta_{3'}| < 0.8$ . The HERWIG predictions (points) are compared with NJETS predictions (histograms), and the phase-space predictions (curves) for (a)  $f_A$ , (b)  $f_B$ , (c)  $X_A$ , and (d)  $\psi'_{AB}$ .

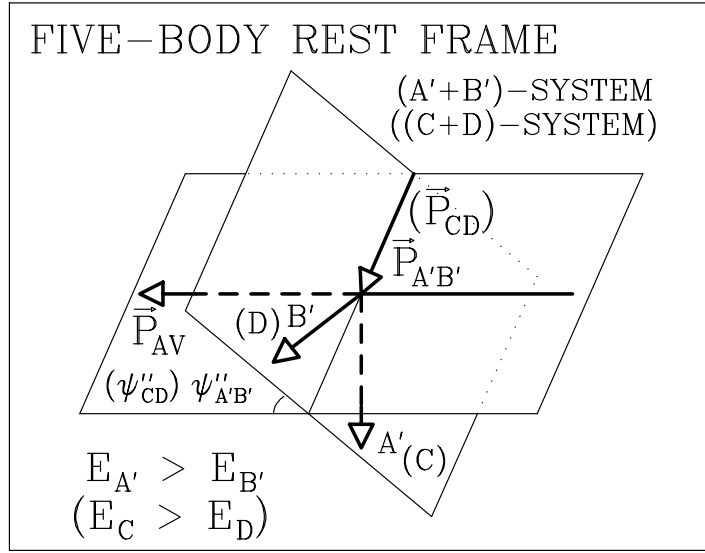
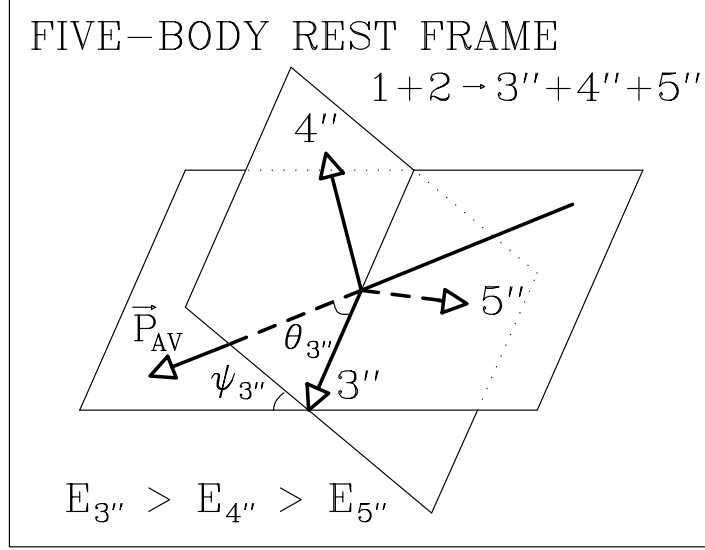


Figure 13: Schematic definition of angles used to describe the five-jet system in the five-jet rest-frame.

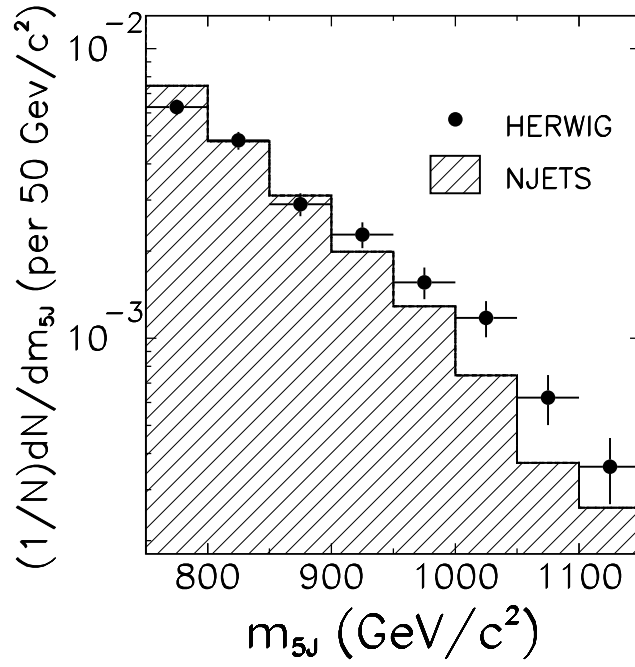


Figure 14: Predicted five-jet mass distributions for five-jet events produced at the Fermilab Proton-Antiproton Collider. HERWIG predictions (points) compared with NJETS predictions (histogram).

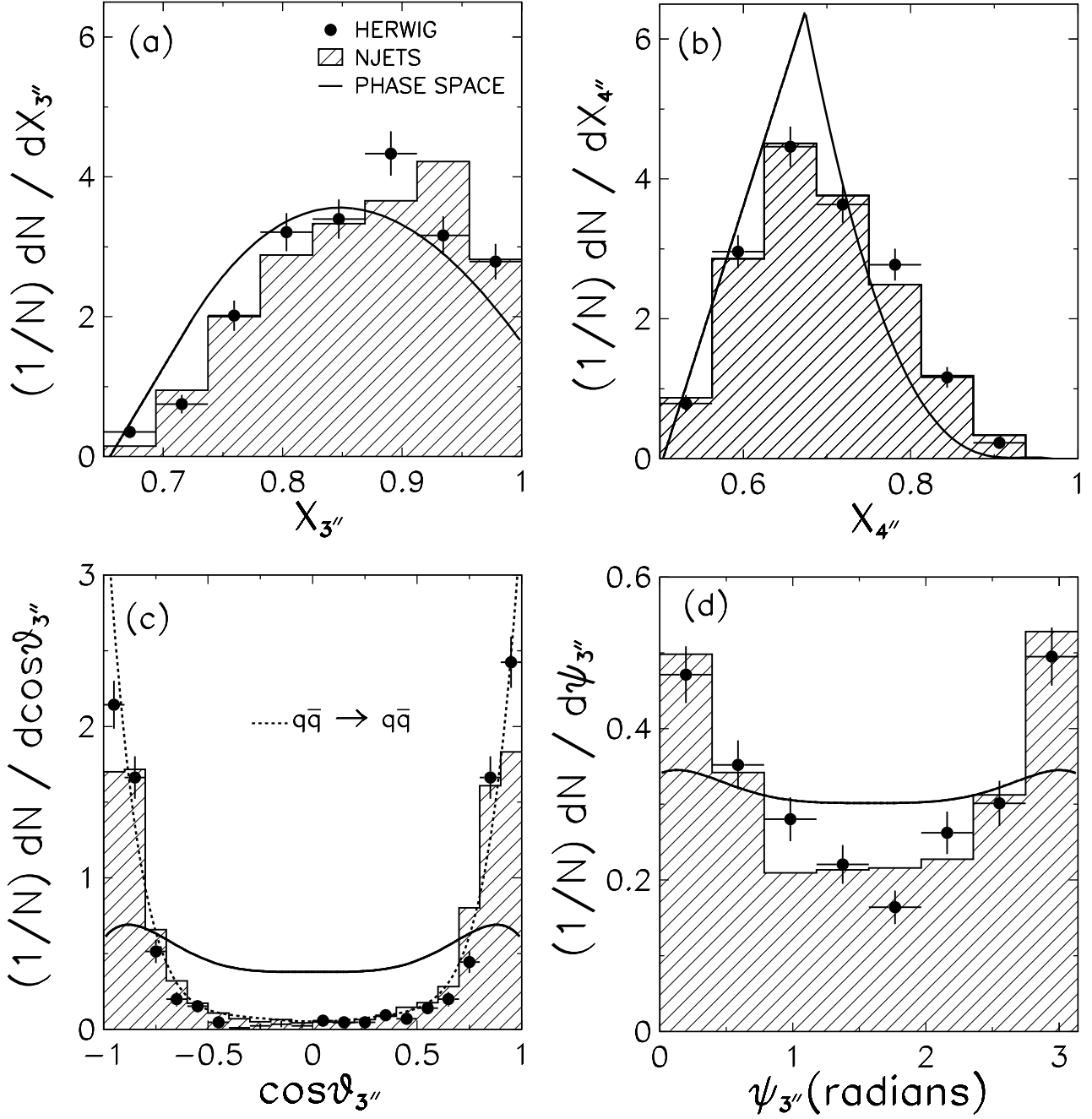


Figure 15: Predicted distributions of three-body variables for five-jet events produced at the Fermilab Proton-Antiproton Collider that satisfy the requirement  $m_{5J} > 750 \text{ GeV}/c^2$ . HERWIG predictions (points) are compared with NJETS predictions (histograms) and the phase-space predictions (solid curves) for (a)  $X_{3''}$ , (b)  $X_{4''}$ , (c)  $\cos \theta_{3''}$ , and (d)  $\psi_{3''}$ . The broken curve in the  $\cos \theta_{3''}$  figure is the LO QCD prediction for  $q\bar{q} \rightarrow q\bar{q}$  scattering.

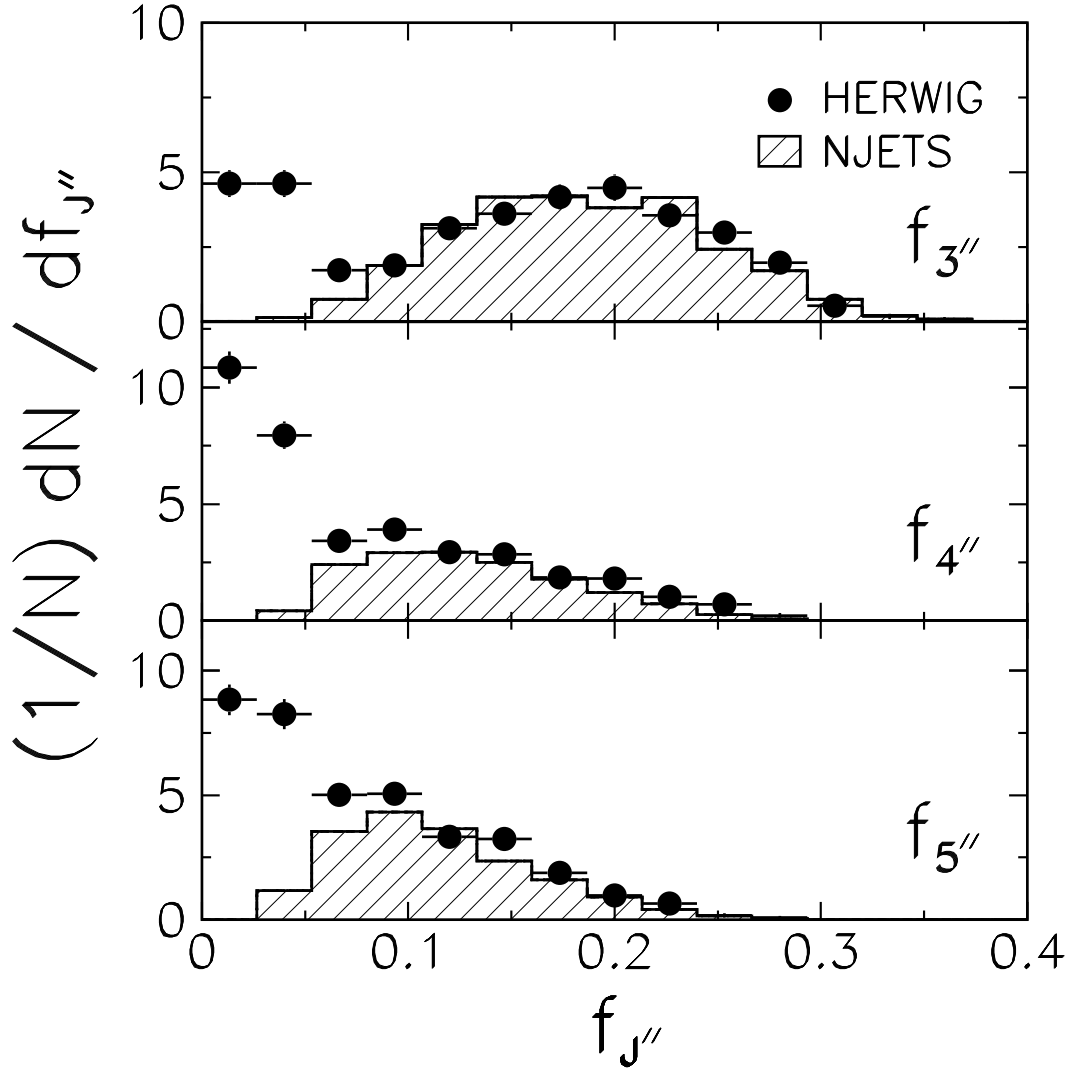


Figure 16: Predicted distributions of the mass fractions described in the text for five-jet events produced at the Fermilab Proton-Antiproton Collider that satisfy the requirement  $m_{5J} > 750 \text{ GeV}/c^2$ . HERWIG predictions (points) compared with NJETS predictions (histograms).



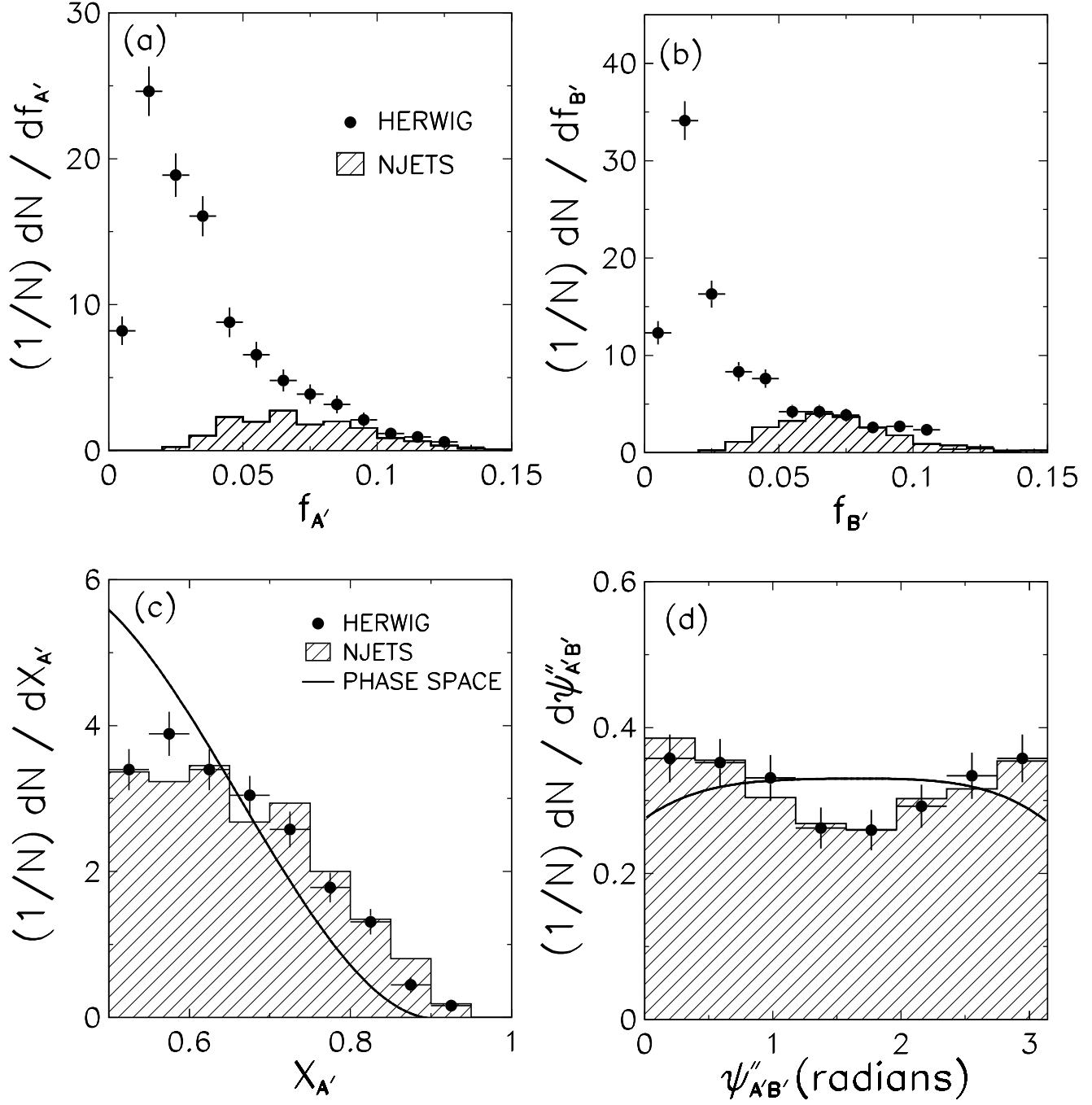


Figure 17: The predicted distributions of the variables describing the  $(A'B')$ -system for five-jet events produced at the Fermilab Proton-Antiproton Collider that satisfy the requirement  $m_{5J} > 750 \text{ GeV}/c^2$ . HERWIG predictions (points) are compared with NJETS predictions (histograms) and the phase-space model predictions (curves) for (a)  $f_{A'}$ , (b)  $f_{B'}$ , (c)  $X_{A'}$ , and (d)  $\psi'_{A'B'}$ .

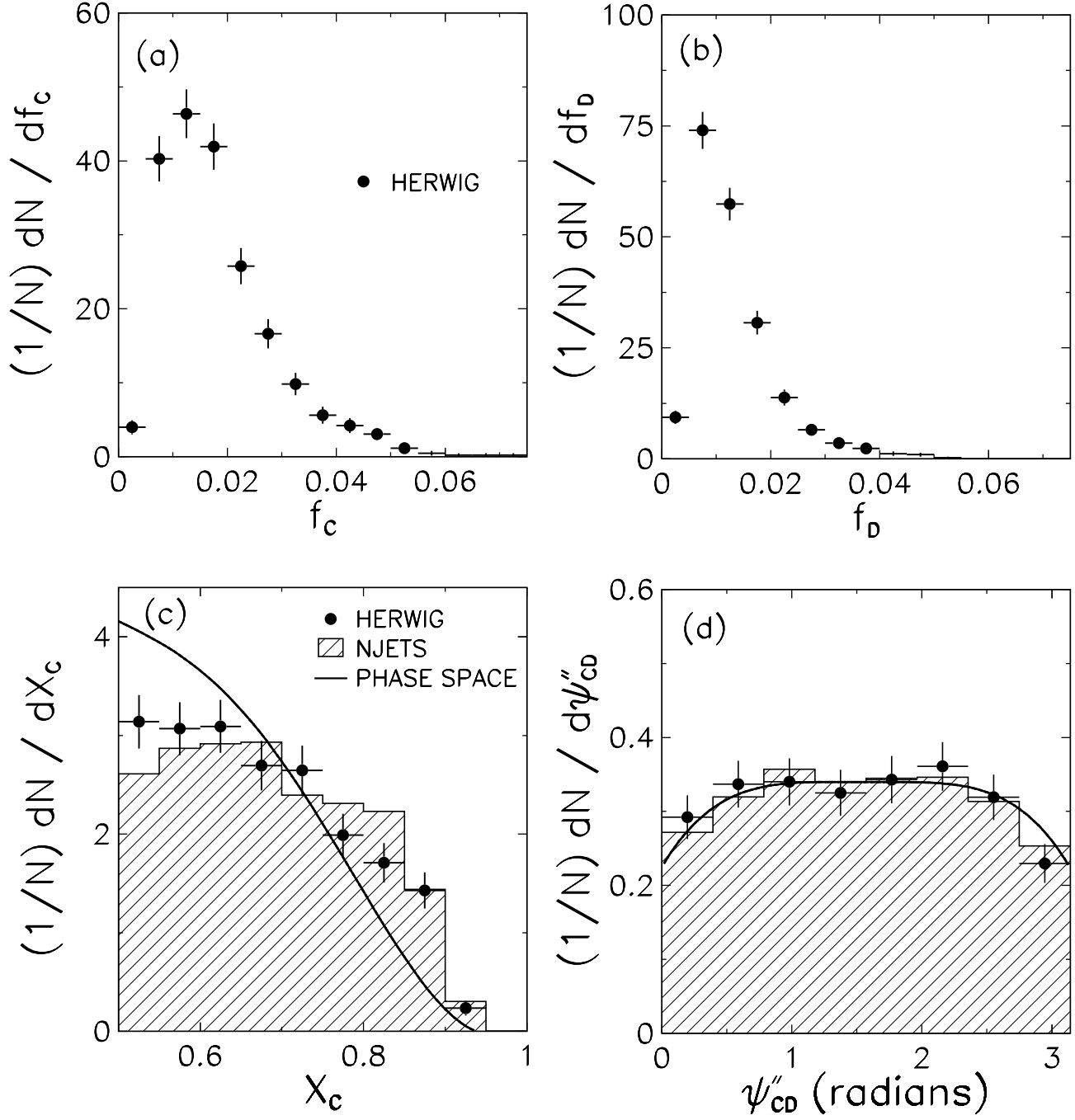


Figure 18: The predicted distributions of the variables describing the (CD)-system for five-jet events produced at the Fermilab Proton-Antiproton Collider that satisfy the requirement  $m_{5J} > 750 \text{ GeV}/c^2$ . HERWIG predictions (points) are compared with NJETS predictions (histograms) and the phase-space model predictions (curves) for (a)  $f_c$ , (b)  $f_D$ , (c)  $X_c$ , and (d)  $\psi''_{CD}$ .